Corrosion of discontinuous reinforcement in concrete subject to railway stray alternating current

Kangkang Tang kangkangtang@gmail.com

College of Engineering, Design and Physical Sciences, Brunel University London, UK

Abstract

Alternating current (AC) traction power systems account for 64% of the UK electrified railway network. However, the investigation of stray AC induced corrosion in reinforced segmental lining tunnels is still very limited. Electrochemical modelling and numerical simulation, validated by the experimental data, indicate that the severity of stray AC induced steel reinforcement corrosion mainly depends on the AC current density, frequency and the chloride content in concrete. Concrete containing discontinuous steel fibres has an inherent corrosion resistance to stray AC attacks due to the electrical double layer developed on the steel surface; the presence of chloride ions in the concrete pore solution however reduces the corrosion resistance. Special attention is therefore needed for steel fibre reinforced concrete (SFRC) subjected to AC current in the presence of high concentration chloride.

Keywords: Teel fibre reinforced concrete; EIS; Potentiostatic; Galvanostatic; Passivation; Depassivation; FEM

List of notations

A	Exposed anode area of a working electrode (cm^2)
β_a, β_b	Anodic and cathodic Tafel constants/gradients
C_f	Steel passive layer capacitance CPE ($S \cdot s^n \cdot cm^{-2}$)
C_{dl}	Double layer capacitance CPE ($S \cdot s^n \cdot cm^{-2}$)
C	Capacitance (μF)
E_{corr}	Corrosion potential (V)
E_{pass}	Steel passivation potential (mV)
E_{pit}	Steel pitting potential (mV)
I_0	Amplitude of the AC current (A)

I_a, I_c	Anodic and cathodic currents (A)
I_{corr}	Corrosion current (A)
i_{corr}	Corrosion current density (A/cm^2)
i_s	Stray current (A)
i_T	Railway traction current (A)
L	Distance between adjacent railway substations (m)
R_s	Resistance of the solution ($\Omega \cdot$cm^2 or Ω)
R_f	Membrane resistance ($\Omega \cdot$cm^2 or Ω)
R_{ct}	Charge transfer resistance of the steel (k$\Omega \cdot$cm^2 or kΩ)
r_R	Running track resistance (Ω)
r_T	track-earth resistance (Ω)
θ	Phase shift (rad)
ω	Angular velocity ($\omega = 2\pi f$, rad/sec)

1 Introduction

The use of discontinuous steel reinforcement such as steel fibres in railway engineering can be traced back to the 1970s when steel fibre reinforced shotcrete (spay concrete) was used in railway tunnel construction [1]. The application of steel fibres in precast segmental linings was much later: the first steel fibre reinforced segmental lining tunnel was the London Heathrow Airport baggage tunnel built in 1995 [2]; the first large-scale application of steel fibre reinforced concrete (SFRC) segments was the Channel Tunnel Rail Link project in 2003 [3].

Previous investigations indicate that discontinuous steel reinforcement in concrete can pick up and transfer stray direct current (DC) [4]. The chloride threshold level for corrosion of steel fibres in concrete is however much higher than that of conventional steel reinforcement, indicating enhanced corrosion resistance of SFRC. For an electrified railway system, the transmission of power is normally provided by an overhead wire or a conductor rail. Stray current refers to the electric current which disperses from the current return path, i.e. the running track, to surrounding buildings and infrastructures. The presence of chloride ions in surrounding soil leads to the breakdown of steel passivation in conjunction with a reduced corrosion potential, $E_{active, corr}$. Its voltage difference in comparison to passive steel ($E_{passive, corr}$) is the primary driving force of the macrocell which allows electrons to travel from the anode to cathode through the steel reinforcement cage. Stray direct current (DC) can further enhance the electrochemical reactions by shifting the electrode potential in a positive direction. It is a legal requirement for electrified railway and tramway promoters to demonstrate, mitigate and manage the stray current risk to a level that can be accepted by all parties who have concerns about their underground apparatus. BS EN 50122-2 [5], provisions against the effects of stray currents caused by DC traction systems, provides comprehensive advice on the design and management of electrified railway. The fundamental principles to limit the risk of stray DC current include: 1) increase the rail-to-earth resistance and 2) reduce the resistance of the return current path.

In comparison to the stray DC induced corrosion, stray AC induced corrosion has only been reported ~~more recently~~ since the 1980s, alongside the development of high-speed rail. For instance, serious corrosion was identified on the surface of buried pipelines in parallel with a 15 kV AC powered railway in Germany in 1986 [6]. Thereafter, more cases of stray AC attacks to pipelines were reported in France and North America [7,8]. Bertolini et al. [9] reported that an AC density of 5 mA/cm^2 gave rise to a noticeable increase in the macrocell current between the excited steel reinforcement and passive steel embedded in concrete containing 0.4% chloride (% mass of cement). Kuang and Cheng [10] suggested a similar AC threshold current density of 3 mA/cm^2 for steel corrosion in concrete. It should be noted that AC current densities might not be the only parameter governing the severity of AC-induced steel corrosion. Previous investigations on pipelines reported that serious corrosion did not always occur in places where the highest AC current density leakage was expected [11]. Other factors such as pH and chloride levels need to be taken into account when determining the AC threshold current density.

A critical chloride level or chloride threshold value, which is usually expressed as a percentage (by mass of cement) or a molar ratio between chloride and hydroxide ions in the concrete pore solution, is used to define the chloride content required for depassivation of steel reinforcement. The depassivation of steel can be assessed through visual observation, e.g. visible deterioration occurs on the steel surface [12]. As the depassivation of steel is always associated with the decrease in corrosion potential (E_{corr}), measurements of E_{corr} can be taken as a quantitative approach to determine the chloride threshold level for corrosion of steel reinforcement in concrete. For instance, Brenna [13] determined the critical chloride content when a decrease of 0.50 V was observed in the measured E_{corr}. In addition to E_{corr}, Bertolini [14] directly measured pitting potential (E_{pit}) of steel exposed to different chloride levels, upon which the critical chloride level of each E_{pit} was determined. A great variability was however observed in measured E_{pit} and this was attributed to the stochastic nature of steel pitting corrosion [14]. Steel corrosion is primarily a result of the anodic current (I_a) according to Faraday's laws of electrolysis: the amount of substance which reacts or literates is directly proportional to the quantity of electric charge passing through it. A chloride content required for a corrosion current density ($i_{corr} = I_{corr}/A$) equal or greater than 0.2 μA/cm^2, which is equivalent to a corrosion rate (CR) of 0.0023 mm/year, has been used for the determination of the critical chloride content or the chloride threshold [14]. Corrosion current (I_{corr}) can be evaluated by conducting a Tafel polarization test [15]. A nonlinear regression analysis can be conducted to determine I_{corr} based on E-I curves obtained using Butler-Volmer equation:

$$I = I_{corr} \left[\exp\left(\frac{E - E_{corr}}{\beta_a} \right) - \exp\left(-\frac{E - E_{corr}}{\beta_c} \right) \right]$$

(1)

In summary, visual observation and the measurement of E_{corr} or E_{pit} can be taken as a fast-track approach to qualitatively assess the severity of chloride attacks but they cannot provide information about the steel passivation behaviour or the corrosion speed. In this work, i_{corr} of steel fibres, under different working conditions, was determined through a regression analysis. This is discussed in Section 3.1.

The corrosion of steel reinforcement in concrete under a stray current environment is of an electrochemical nature as discussed. Instrumental methods for electrochemistry are widely used for the determination of the corrosion behaviour of steel fibres based on the use of either aqueous electrolytes such as simulated concrete pore solutions or a solid electrolyte such as mortar or concrete. Mortar (or cement paste) is a cementitious composite between cement, water and sand and it can represent the structure of concrete which also contains coarse aggregate such as limestone and gravel. In comparison to mortar, a simulated concrete pore solution is cost effective and easier to prepare and manipulate [4,16]. The application of a simulated concrete pore solution for the study of reinforcement corrosion in concrete can be traced back to 1949 when Pourbaix [17] measured polarization curves of steel immersed in a saturated $Ca(OH)_2$ solution. The measurement of electrical properties of steel reinforcement in concrete such as polarization resistance (R_p) was conducted much later in the 1970s [18]. In addition to the polarization test, the use of more advanced electrochemical techniques including electrochemical impedance spectroscopy (EIS) have been popularly used nowadays due to the additional information it can provide, e.g. dialect properties of concrete and characteristics of the steel passivation layer [18]. EIS was conducted in this project based on the use of both aqueous and solid electrolytes. This is discussed in Section 2.4 and 2.5.

In addition to electrochemical analyses, numerical simulation based on finite element modelling (FEM) has been increasingly used to study corrosion in reinforced concrete structures. For instance, Brenna et al. [19] modelled the electric current field developed in a segmental lining tunnel under a stray DC current environment and a high stray current density was identified at the interface between adjacent segmental rings. Hong et al. [20] investigated the electric current field developed in a railway viaduct subjected to a stray DC current through FEM and a high stray current density was noted at the pier-deck interface. These studies provide useful information about the stray current distribution inside a structure, upon which an effective corrosion monitoring system can be implemented. In addition to the modelling of the electric field, Laurens et al. [21] investigated macrocell corrosion in a steel reinforced concrete specimen through FEM. The polarization behaviour of steel reinforcement (or the E-i curves) was defined by the Butler-Volmer equation (Eq. (1)). This approach was based on constant polarization parameters (e.g. β_a and β_c) and both anodic and cathodic reactions are kinetically controlled. This steady-state analytical approach however may lead to biased results for the predicted corrosion current (i_{corr}) due to the constant β_a and β_c values assumed. It cannot consider the possible diffusion limited reactions such as the reduction of oxygen at the cathode either. Due to these limitations, FEM was conducted in this project, as detailed in Section 2.6, to study the electric field developed in an electrolytic cell (i.e. test 4.1), upon which an electrochemical model was developed.

2 Experimental and analytical procedures

The primary objective of this work was to justify whether discrete and discontinuous steel fibres can pick up stray AC currents and lead to similar corrosion attacks as occur under a stray DC environment. This was achieved through stray AC polarization using both aqueous (Section 2.2) and solid electrolytes (Section 2.3). The corrosion behaviour of steel fibres without the presence of stray currents was investigated through Tafel polarization and this is discussed in Section 2.1.

In terms of the modelling of a stray AC environment, both potentiostatic and galvanostatic polarization techniques had been previously used based on a review of the literature [22–25]. Potentiostatic polarization can simulate a stray current by controlling electric voltage (V); galvanostatic polarization is through controlling electric current (A). It should be noted that a constant AC voltage cannot ensure a constant driving voltage applied to steel reinforcement due to the fluctuation of electrode potential with time. Previous studies also indicate that the magnitude of stray current (i_S) is a function of railway traction current (i_T), resistance of the running tracks (r_R), track-earth resistance (r_T) and the distance between substations (L), as seen in Eq. (2) [26]. Or alternatively, a constant value of i_S is expected if a standard track-and-earth insulation (r_T) is provided and the distance between adjacent substations (L) is maintained.

$$i_S = \frac{1}{12} i_T \frac{r_R}{r_T} L^2$$

(2)

This has been followed in this work and controlled-current (galvanostatic) polarization was adopted to simulate stray AC interference.

2.1 Study 1: Corrosion behaviour of steel fibres without the presence of stray current

The steel fibres used in this work are 62 mm long, 0.75 mm in diameter cold drawn steel fibres with hooked ends, as seen in Fig. 2. Steel fibres were ground by 2000 grit emery paper prior to testing. To prevent galvanostatic corrosion, steel fibres were prewired and the connection was coated with a hot melt polymer adhesive. The exposed area of the wired steel fibre was approximately 1.4 cm^2.
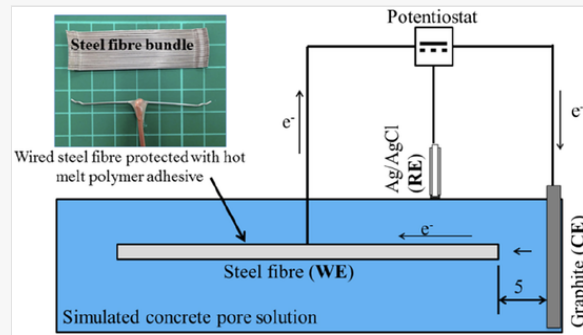
alt-text: Fig. 1

Fig. 1
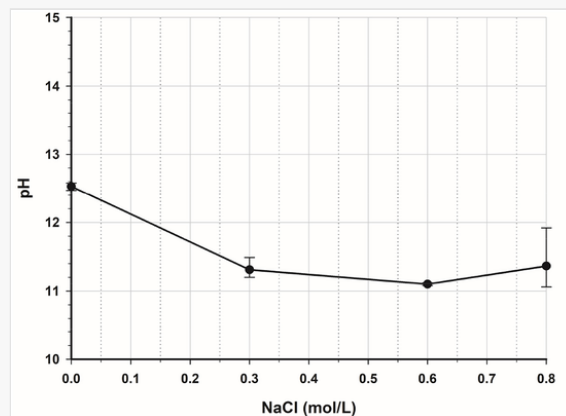
pH of simulated concrete pore solutions.

alt-text: Fig. 2

Fig. 2

Test 1: 3-electrode Tafel polarization test (all units in mm).

A 3-electrode electrochemical cell, as seen in Fig. 2, was developed for the Tafel polarization test. The prewired steel fibre was used as the working electrode (WE) and its electrode potential against a silver/silver chloride (Ag/AgCl, with filling solution 3% KCl) reference electrode (RE) was measured by placing the RE on the top surface of a high density upholstery foam beam which approximates the porous structure of a concrete specimen. The upholstery foam beam soaked up the simulated pore solution, i.e. saturated $Ca(OH)_2$; the effect of chloride on the corrosion of steel fibres was investigated by adding reagent grade NaCl into the electrolyte at different concentrations, i.e. 0, 0.3, 0.6 and 0.8 mol/L 0.6 mol/L NaCl represents the salinity of seawater [27]. It should be noted that chloride contents near the steel surface may increase with time due to the diffusion of chloride ions alongside the anodic reaction ($Fe \rightarrow Fe^{2+} + 2e^-$) [14]. For a railway tunnel, it might be essential to consider a higher chloride level due to an extended service life of 100 years or more. In comparison, an ordinary building which has a 50 year design life only. As an example, both HS2 and Crossrail tunnels in the UK have a design life of 120 years. To address the long design life of a railway tunnel and associated transport mechanism of chlorides, a chloride level up to 0.8 mol/L was considered in this project. The pH of the concrete pore solutions was assessed using a Phidget pH sensor and results are shown in Fig. 1 pH was found to range between 11.2 and 12.6. The latter is similar to that reported for ordinary steel reinforced concrete, i.e. about 12.5 [4].

Tafel polarization was conducted by scanning a DC voltage, 1 mV/s, between the WE and a 40 × 50 × 3 mm graphite plate which performs as a counter electrode (CE) using a Gamry Interface 1000E potenitostat. Such a slow potential scanning rate allows the nonlinear correlation between externally applied potential (E) and the resulting current density i ($i = I/A$) response to be measured.

- **Test 1**: Tafel polarization test of steel fibres using simulated concrete pore solutions containing different chloride levels (0, 0.3, 0.6 and 0.8 mol/L).
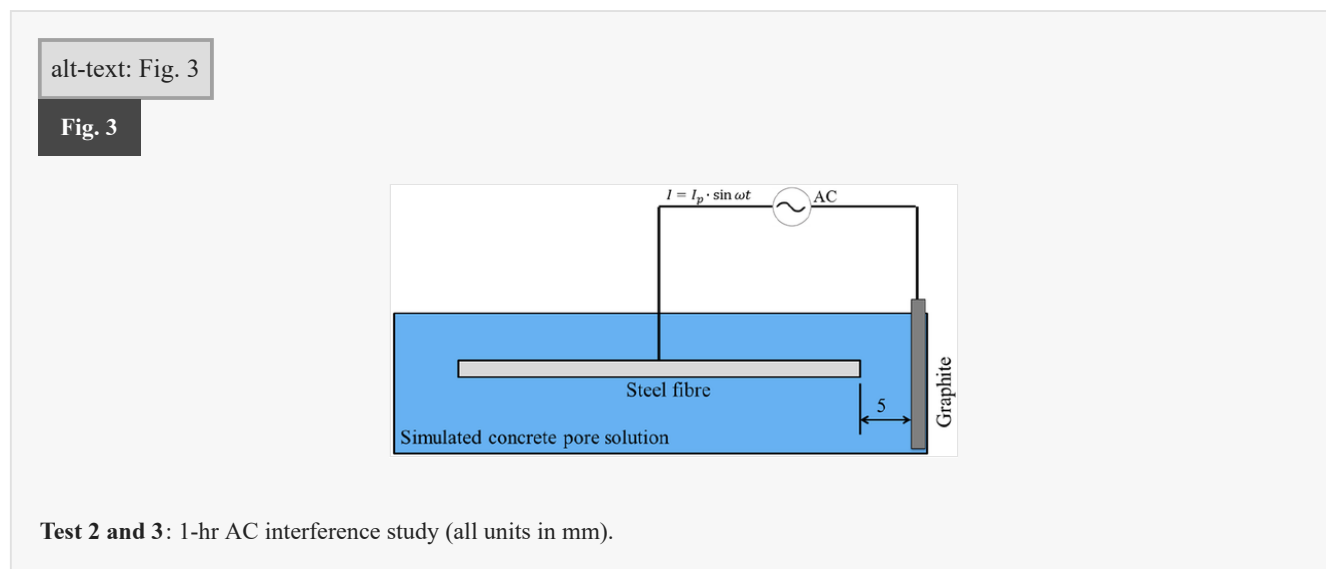
Three parallel samples were prepared and tested in each group. Freshly prepared electrodes and electrolytes were used in each test. Tafel polarization results were analysed through a nonlinear regression to determine the corrosion current density (i_{corr}) and corrosion potential (E_{corr}). Test results are discussed in Section 3.1. As steel corrosion is a thermally activated process and affected by the ambient temperature variations, all

experiments discussed in this paper were conducted inside an environmental chamber which was set at a constant temperature (20 °C) and humidity (90%).

2.2 Study 2: Effects of chloride on the corrosion of steel fibres under stray AC environments

In order to study the effect of AC currents and chloride ions on the corrosion behaviour of steel fibres, **test 2** was conducted by applying a constant AC current, i.e. I_0 = 60 mA, to a prewired steel fibre embedded in an electrolytic cell as shown in Fig. 3.

- **Test 2**: Study of the effect of electrolyte chloride levels (0, 0.3, 0.6 and 0.8 mol/L) on the corrosion behaviours of steel fibres subjected to a constant AC current ($I = I_0 \cdot \sin \omega t$; $I_0 = 60 \ mA \ and \ \omega = 50 \ Hz$).

alt-text: Fig. 3

Fig. 3

$I = I_p \cdot \sin \omega t$ AC

Steel fibre

5

Graphite

Simulated concrete pore solution

Test 2 and 3: 1-hr AC interference study (all units in mm).

This was achieved using the Gamry Interface 1000E potentiostat with a Gamry's Virtual Front Panel (VFP600) software package which allows the potentiostat to perform as a galvanostat and drives a constant alternating current (AC) between the working and auxiliary graphite electrode. The magnitude of the AC current, i.e. 60 mA, was adopted based on a review of the literature [13]. The AC frequency was the same as the UK National Grid AC frequency, i.e. 50 Hz. After 1-hr AC polarization, the tested steel fibre was ringed using deionized water before the Tafel polarization test was conducted to determine E-i curves, upon which i_{corr} and E_{corr} were determined; simulated concrete pore solution, i.e. saturated $Ca(OH)_2$, was used as the electrolyte. Results are discussed in Section 3.2.

2.3 Study 3: Effects of stray AC current values on the corrosion of steel fibres

In order to study the effect of AC current densities on the corrosion behaviour of steel fibres, **test 3** was conducted by applying different AC currents (I_0), i.e. 30, 60 and 90 mA, to the same electrochemical cell as seen in Fig. 3, using freshly prepared steel fibres and electrolytes. After **test 3**, the tested steel fibre was ringed using deionized water before the Tafel polarization test was conducted to determine E-i curves, upon which i_{corr} and E_{corr} were determined. Results are discussed in Section 3.2.

-

Test 3: Study of the effect of AC currents ($I = I_0 \cdot \sin \omega t$, $I_0 = 30, 60 \text{ and } 90 \, mA$, $\omega = 50 \, Hz$) on the corrosion behaviours of steel fibres in simulated concrete pore solution containing 0.3 mol/L NaCl.

A constant chloride level, 0.3 mol/L, was used and it represents the salinity of underground soil measured during the construction of the service tunnel in Copenhagen where steel fibres were used as the primary reinforcement material [28].
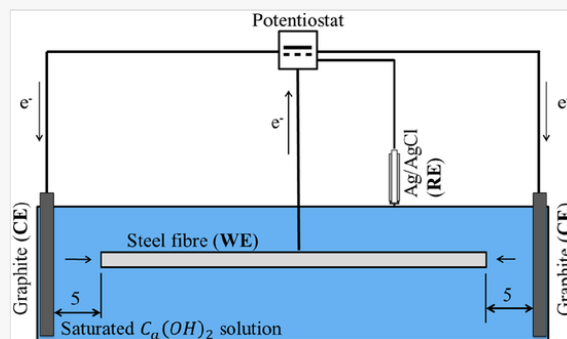
2.4 Study 4: Ability of discrete steel fibres to pick up and transfer AC currents (use of simulated concrete pore solutions)

In order to justify whether discrete and discontinuous steel fibres can pick up and transfer AC currents, **test 4.1** was conducted using an electrochemical cell as seen in Fig. 4. **Test 4.1** also allowed the investigation of AC frequencies and their effect on the ability of discrete steel fibres to pick up and transfer AC currents.

- **Test 4.1**: Study of AC frequencies ($I = I_0 \cdot \sin \omega t$, $I_0 = 60 mA$, $\omega = 20, 50 \text{ and } 100 Hz$) and their influence on the ability that discrete steel fibre picks up AC currents. A simulated concrete solution containing 0.3 mol/L NaCl was used.

alt-text: Fig. 4

Fig. 4
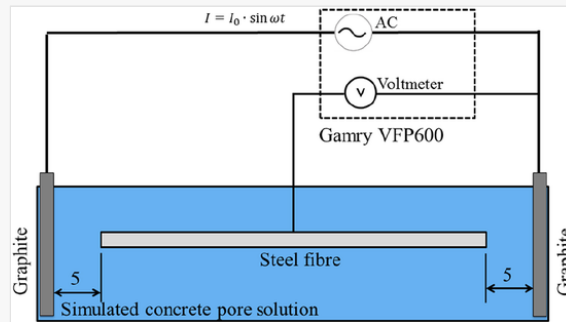
Test 4.1: Measurement of stray AC current picked up by the discrete steel fibre (all units in mm).

The Gamry Interface 1000E potentiostat with the Gamry's Virtual Front Panel (VFP600) software package allows the potentiostat to perform as a galvanostat which drives constant AC currents between the two auxiliary graphite electrodes, simultaneously measuring voltage drop between the steel fibre and the graphite auxiliary graphite electrode. Such an experimental setup allows for the determination of stray AC currents picked up and transferred by the discrete steel fibre. This discussed in Section 3.3.

After **test 4.1**, the tested steel fibres were ringed using deionized water before the electrochemical impedance spectroscopy (EIS) test, or **test 4.2**, was conducted using the electrochemical cell shown in Fig. 5. As steel corrosion due to AC positive cycles may occur on both sides of a steel fibre, two counter electrodes (CE) were used, allowing for the measurement of the corrosion state on both sides of the steel fibre. In comparison to a

standard Tafel polarization test, a smaller potential perturbation (E_0), ±25 mV (vs OCP), was adopted by EIS. A sinusoidal AC potential $E_0 \cdot \sin(\omega t)$, at frequencies varying between 10^5 and 10^{-1} Hz, was swept between the WE and RE. The impedance of the electrochemical cell was determined as the correlation between the applied potential (E) and the measured current density (i). The interpretation of EIS data was based on the best-fit results obtained through equivalent electrical circuit modelling. The results are discussed in Section 3.3.

alt-text: Fig. 5

Fig. 5

Test 4.2: 3-electrode EIS test – use of aqueous electrolyte (all units in mm).

2.5 Study 5: Ability of discrete steel fibre to pick up and transfer AC currents (use of solid electrolytes)

The use of simulated concrete pore solutions allows for a quick assessment of the electrical resistivity, conductivity and corrosion resistance of steel fibres. On the other hand, simulated concrete pore solutions might not be able to fully represent the real working conditions of reinforcing steel such as the oxygen content, pH and steel-concrete interface conditions. The resistivity of concrete also affects the anodic behaviour (β_a) of steel which in turn affects its corrosion rate. The hydrolysis of anodic products due to the anodic reaction may lead to the acidity near the steel surface: $F_e^{2+} + 2H_2O \rightarrow F_e(OH)_2 + 2H^+$. The acidity effect alongside the chloride ions diffused to the steel surface enhances the corrosion of steel reinforcement. Neither of above effects can be sufficiently considered by using simulated concrete pore solutions. In order to verify that results obtained using simulated concrete pore solutions (i.e. **test 4.1**) can be applicable for SFRC, **test 5.1** was conducted and mortar was used as the electrolyte.

- **Test 5.1**: 24-hr study of the effect of solid electrolytes (mortar) on the age of 3 days after casting, with and without the presence of chlorides (e.g. 0 and 2% NaCl by mass of cement), subject to a constant AC current ($I = I_0 \cdot \sin \omega t$; $I_0 = 10 \, mA$; $\omega = 50 \, Hz$)

A steel fibre, pre-connected to a copper cable and coated with a hot melt polymer adhesive, was embedded into freshly mixed mortar as the WE. The mix proportions are shown in Table 1. The effect of chloride ions on the corrosion behaviour of SFRC was investigated by adding 0 and 2% NaCl (by mass of cement) into the

mortar mixes. Two graphite plates, 40 × 50 × 3 mm, were placed on both sides of the WE as the auxiliary electrode.

Mortar mix proportions.

Mortar mixes	CEM I 52,5 (kg/m^3)	Free W/C	Sand (0–4 mm) (kg/m^3)	NaCl (kg/m^3)
0%NaCl	480	0.35	1814	0
2%NaCl	480	0.35	1814	9.6

The Gamry galvanostat used in this project has an AC voltage limit of 10 V. A reduced AC current (I_0), i.e. 10 mA, was used in **test 5.1** to avoid overloading the galvanostat. On the other hand, the use of mortar as the solid electrolyte enabled a long-term stray AC current simulation with less concerns about the evaporation effect and associated salinity variations as occurs in aqueous electrolytes. After **test 5.1**, the electrochemical impedance spectroscopy (EIS) test, i.e. **test 5.2**, was conducted using the same electrochemical cell (Fig. 6) but with an Ag/AgCl reference electrode (RE) placed on the top of the mortar. A potential perturbation (E_0), ±25 mV (vs OCP), was adopted and a sinusoidal AC potential $E_0 \cdot \sin(\omega t)$, at frequencies varying between 10^5 and 10^{-1} Hz, was swept between the WE and two graphite electrodes (CE). The impedance of the electrochemical cell was determined as the correlation between the applied potential (E) and the measured current density (i). The interpretation of EIS data was based on the best-fit results obtained through equivalent electrical circuit modelling and this is discussed in Section 3.3 (see Fig. 7).

alt-text: Fig. 6

Fig. 6
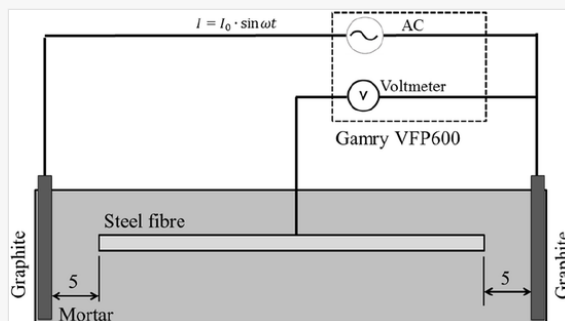
Test 5.1: Measurement of stray AC current picked up by the discrete steel fibre (all units in mm).

alt-text: Fig. 7

Fig. 7
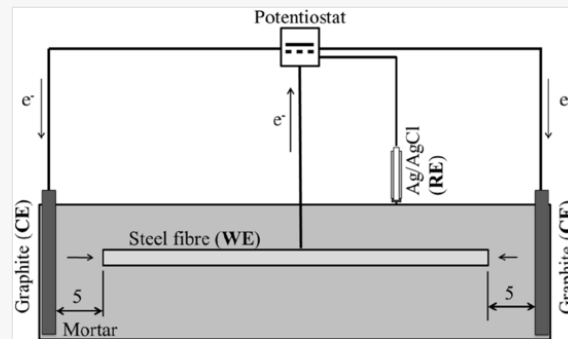
Test 5.2 3-electrode EIS test – use of solid electrolyte (mortar) (all units in mm).

2.6 Study 6: Finite element modelling (FEM)

The purpose of FEM was to have a better understanding of the electric field developed in a SFRC specimen subjected to stray AC currents. The electrolytic cell adopted in **test 4.1** (Fig. 4) was modelled using ANSYS, a multi-physics finite-element software package. Both electrolyte and graphite electrodes were meshed into 1×1 mm PLANE230 elements which is a 2D, 8-node and current-based electric element. The embedded steel fibre was also meshed into 2D PLANE230 elements in a π shape, with a total length of 62 mm and 1 mm in the thickness, approximating the profiled shape of the steel fibre used. The electrical resistivity of steel, graphite and electrolyte (i.e. 0.3 mol/L NaCl) was taken as 4.6×10^{-7}, 2.5×10^{-6} and 0.2 Ω m based on a review of the literature [29]. A constant AC current ($I_0 = 60mA; \omega = 50 \, Hz$), as used in **test 4.1**, was applied between the graphite electrodes. A transient electric analysis was conducted and FEM results are discussed in Section 3.3 (see Fig. 8).

3 Results and discussion

3.1 Corrosion behaviour of steel fibres without the presence of stray current

Test 1, i.e. Tafel polarization, provided useful information about the electrochemical performance of steel fibres under a variety of chloride levels, simulating different working conditions of concrete. Tafel polarization results were presented as curves between the electrode potential E (vs Ag/AgCl RE) and the current density i ($i = I/A$) on a logarithmic scale, as seen in Fig. 9. A represents the exposed surface area of the steel fibre to the electrolyte, i.e. 1.4 cm^2. A nonlinear regression analysis based on Butler-Volmeter equation (Eq. (1)) was conducted to determine i_{corr} and corrosion potential (E_{corr}) using the Gamry Echem Analyst software package [30]. The best-fit results for i_{corr} and E_{corr}, as seen in Fig. 10, indicate that E_{corr} shifts more negatively due to the presence of chloride ions. Alongside a reduction in E_{corr}, i_{corr} increases steadily from 0.2 µA/cm^2 under a chloride-free condition to 1.2 µA/cm^2 with 0.8 mol/L in the electrolyte, showing high

susceptibility of steel pitting. In summary, the intensity of steel fibre corrosion, without the presence of an external electric potential, is governed by the salinity of the electrolyte: the higher salinity in the electrolyte, the higher susceptibility of pitting corrosion.
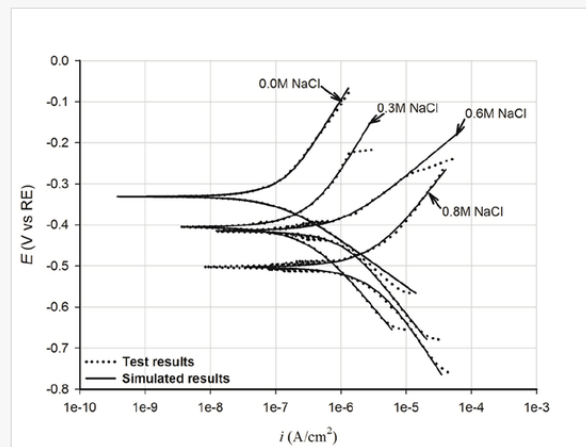

alt-text: Fig. 8

Fig. 8
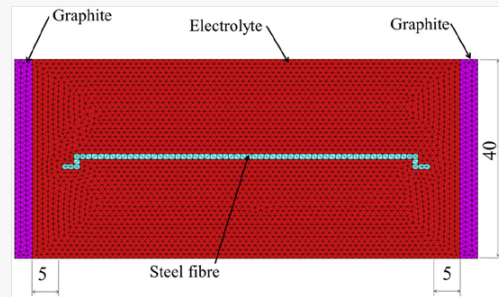
Test 4.1 Finite element modelling (all units in mm).
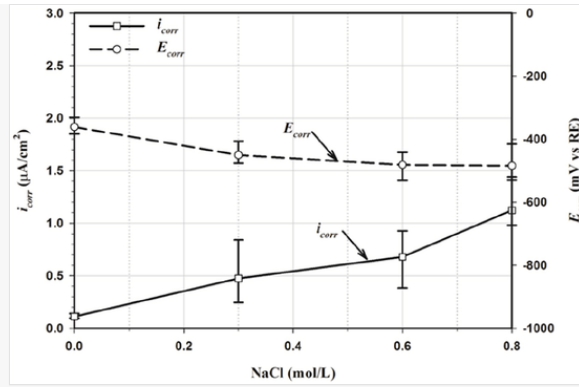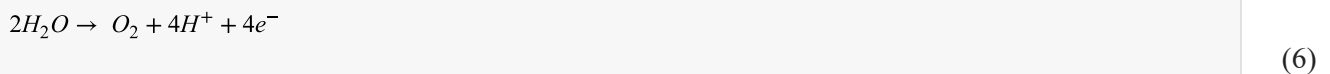

alt-text: Fig. 9

Fig. 9

Test 1 results: effects of electrolyte chloride contents on Tafel polarization curves.

alt-text: Fig. 10

Fig. 10

Test 1 results: effects of electrolyte chloride contents on i_{corr} and E_{corr}.

3.2 Stray AC-induced corrosion of discrete steel fibres

Test 2 and **3** investigated the corrosion behaviour of steel fibres due to the presence of stray AC currents. Similar to **test 1**, different chloride contents, e.g. 0, 0.3, 0.6 and 0.8 mol/L, were added into the electrolyte to consider different working conditions. An external AC voltage allows charged anions and cations in the electrolyte to flow through the bulk solution. The potential difference between the electrode and the bulk solution leads to the exchange of electrons and as such, an electric current is pushed through the entire electrolytic cell. The possible anodic reactions include:

$$F_e \rightarrow F_e^{2+} + 2e^-$$

(3)

$$2Cl^- \rightarrow Cl_2 + 2e^-$$

(4)

$$4OH^- \rightarrow O_2 + 2H_2O + 4e^-$$

(5)

$$2H_2O \rightarrow O_2 + 4H^+ + 4e^-$$

(6)
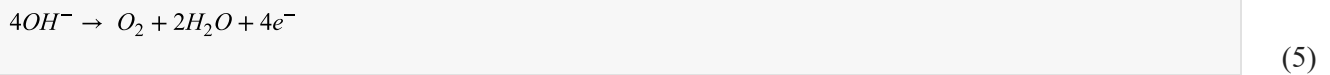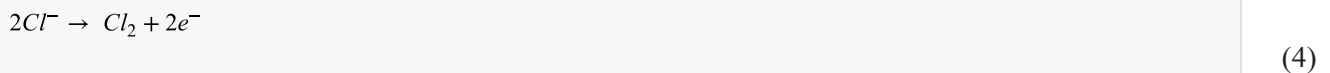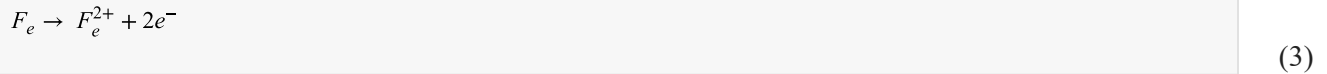
The possible cathodic reactions include:

$$2H_2O + 2e^- \rightarrow H_2 + 2OH^-$$

(7)

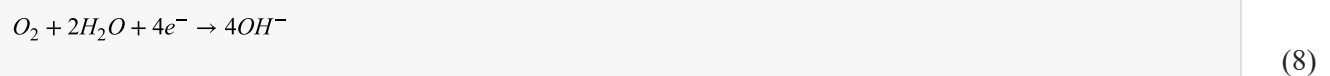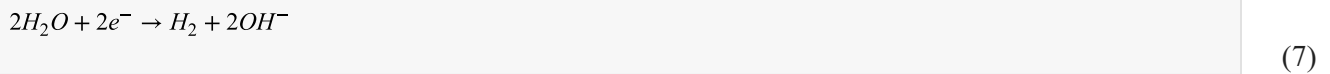$$O_2 + 2H_2O + 4e^- \rightarrow 4OH^-$$

(8)

Fig. 11 shows the Tafel polarization curves after 1-hr AC polarization. A nonlinear regression analysis based on Butler-Volmeter equation (Eq. (1)) was conducted to determine i_{corr} and E_{corr}; results are shown in Fig. 12. The exposure to an AC current did not further reduce E_{corr}, in comparison to those shown in Fig. 9. On the other hand, i_{corr} is over 30 $\mu A/cm^2$ under a high chloride content (i.e. 0.8 mol/L), indicating serious pitting corrosion. In summary, a combined effect of high chloride content (≥ 0.6 mol/L) and an AC environment significantly enhanced steel corrosion. In addition, Fig. 13 shows that AC current density is a governing parameter of steel fibre corrosion: an increase of AC current densities leads to a reduction in E_{corr} and an increase of i_{corr} and this finding agrees with Wang et al. [31].
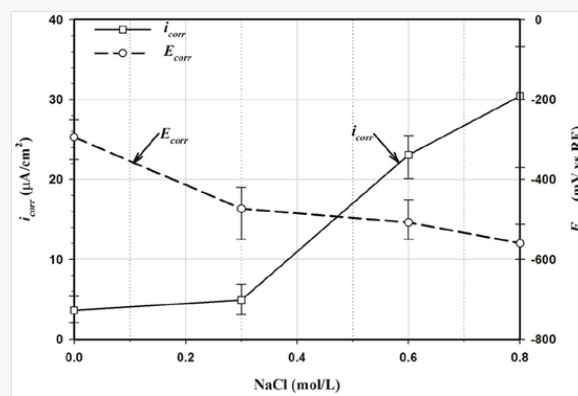
alt-text: Fig. 11

Fig. 11
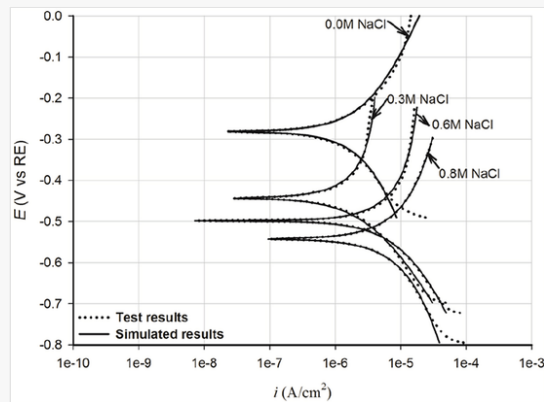
Test 2 results: effects of electrolyte chloride contents on Tafel polarization curves after 1-hr AC interference.
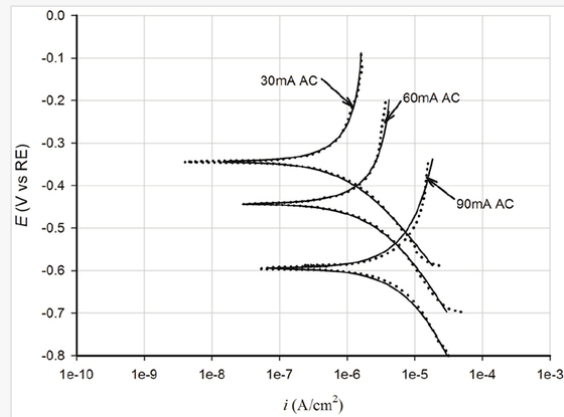
alt-text: Fig. 12

Fig. 12

Test 2 results: effects of electrolyte chloride contents on i_{corr} and E_{corr} after 1-hr AC interference.

Test 3 results: effect of 50 Hz AC current (I_0) on Tafel polarization curves after 1-hr AC interference.

3.3 Effect of discontinuity of steel reinforcement on AC-induced steel fibre corrosion in SFRC

The main objective of **test 4.1** and **5.1** was to justify whether stray AC currents can be picked up and transferred by discontinuous steel fibres. The voltage drop between the steel fibre and auxiliary graphite electrode during **test 4.1** was shown in Fig. 14. It indicates that: 1) there is a constant voltage drop E between the steel fibre and auxiliary electrode which drives electric current through and 2) a lower E is required to drive a higher frequency AC current in comparison to that subjected to a lower frequency AC current. The latter shows that the magnitude of stray AC currents picked by the discrete steel fibre is affected by AC frequencies (ω).
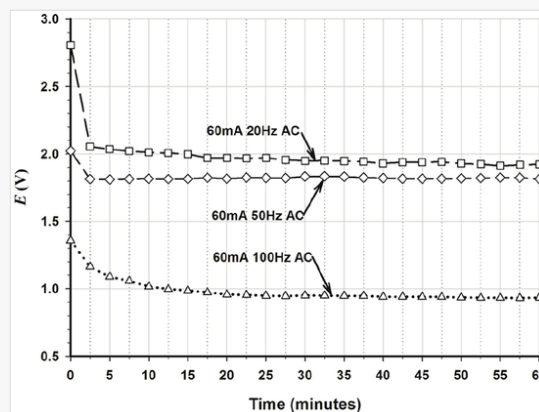
Test 4.1 results: AC voltage drop between steel fibre and auxiliary electrode ($I_0 = 60mA$, $\omega = 20, 50 \; and \; 100Hz$).

The electrolytic process undertaken during **test 4.1** was investigated through FEM and the conduction field is displayed in Fig. 15. The arrows represent the current field developed in each element and their lengths are proportional to the induced current density. Fig. 15 shows that a large percentage of AC current flows through the embedded steel fibre which has a smaller resistivity in comparison to the electrolyte. The peak current density occurs in close proximity to its hooked end and this can be attributed to the greater voltage drop between steel and concrete due to the contact resistance [19]. Due to the skin effect [32], the stray AC current is distributed near the surface of steel, leading to more serious corrosion near the hooked end when electrons leave it. This agrees with the visual observation of the steel fibre specimens after **test 4.1** and the growth of corrosion products mainly focused on the hooked ends. Based on above findings, an electrical circuit model (Fig. 16) was developed to simulate AC induced corrosion processes in **test 4.1** when both anodic and cathodic reactions were under charge-transfer control. It consists of a resistor (R_{ct}) in parallel with a capacitor (C) which represents the admittance of the steel-electrolyte interface consisting of a combination of the admittance of the electrical double layer and the polarization resistance. Solution resistance of the electrolyte is represented as a resistor (R_s). In such a parallel circuit (Fig. 16), the non-Faradaic current I_1, or capacitive current, represents the charged ions (e.g. oxygen molecules) in the electrolyte to compensate for the excess of electrons on the electrodes surface. In contrast to I_1, the Faradaic current, I_2, is a direct measure of the rate of the redox reactions. An integration of I_2 (positive parts only) with respect to time gives a total electric charge, upon which the corrosion rate (CR) can be estimated. According to the parallel circuit theory, a larger percentage of the current always flows through the path of less impedance (Z), just as the FEM results indicate (Fig. 15). For a capacitor, its absolute value ($|Z|$) is inversely proportional to both angular frequency (ω) and capacitance (C).
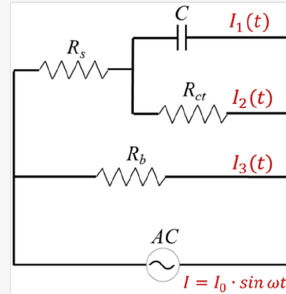
$$|Z| = \frac{1}{\omega \cdot C}$$

(9)

alt-text: Fig. 15

Fig. 15
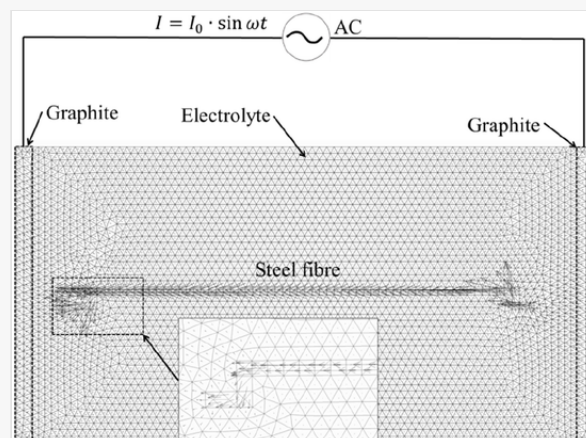
alt-text: Fig. 16

Fig. 16

Equivalent electrical circuit modelling of the steel-electrolyte interface under AC interference.

Eq. (9) shows that an increase of the AC angular frequency (ω) and capacitance (C) leads to a reduction in impedance, allowing more AC currents to flow through the capacitor (C) and thus a higher non-Faradaic current (I_1). Similarly, a reduction in ω allows more Faradaic currents to flow through R_{ct} and thus a higher voltage drop as monitored during **test 4.1** (Fig. 14).

Based on the electrical circuit model discussed above, the Faradaic current, I_2, was solved and shown as Eq. (10). The calculation and validation processes are presented in the Appendix of this paper.

$$I_2(t) = \frac{b}{\sqrt{\omega^2 + a^2}} \sin(\omega t - \theta) + \frac{b \cdot \omega}{\omega^2 + a^2} \cdot e^{-at}$$

(10)

where: $a = \frac{R_b + R_s + R_{ct}}{C \cdot R_{ct} \cdot R_b + R_s \cdot C \cdot R_{ct}}$, $b = \frac{R_b \cdot I_0}{C \cdot R_{ct} \cdot R_b + R_s \cdot C \cdot R_{ct}}$, $\theta = arctan\frac{\omega}{a}$.

Eq. (10) indicates that a reduction in either AC frequencies (ω), charge transfer resistance (R_{ct}) or double layer capacitance (C) will lead to an increase in I_2, or more serious corrosion in the embedded steel. Fig. 14 also shows that a reduced AC voltage drop is required to drive a higher frequency AC current, in comparison to that for a lower frequency AC current. This can be explained according to Ohm's law: an increase in AC frequencies (ω) reduces the Faradaic current (I_2) through the embedded steel and thus the voltage drop. In addition, Fig. 14 shows a major reduction in E, i.e. the voltage drop between steel and auxiliary electrode, in the first 5 min. This indicates the breakdown of steel passivation layer alongside a reduction in charge transfer resistance (R_{ct}) of steel. The detrimental effect of 20 Hz AC, as seen as the reduction in E, is greater than those obtained at 50 and 100 Hz and this also agrees with Eq. (10). It should be noted that ~~the values of~~a constant E ~~were maintained~~value was achieved after approximately 10 min as seen in Fig. 14, indicating a stabilized corrosion state ~~or a constant R_{ct} value has been achieved~~.

The long-term study (e.g. $\geq$ 1hr) of AC polarization based on the use of an aqueous electrolyte might lead to biased results due to the potential evaporation effect and associated salinity variations in the electrolyte. As discussed previously, the steel corrosion rate, with and without the presence of an external voltage, is governed by the anodic current density (i_a) which is related to the potential difference between the anode and cathode (IR_s). In comparison to concrete, the solution resistance (R_s) of an aqueous electrolyte is much smaller. This has been addressed in **test 5.1** by using the solid electrolyte (i.e. mortar). The voltage drop (E) between the steel fibre and auxiliary graphite plate is presented in Fig. 17. It shows that E increases with time without the presence of NaCl, showing increased impedance and corrosion resistance which can be attributed to the maturity of mortar alongside the cement hydration reactions [33]. A combined effect of AC currents and 2% NaCl (% by mass of cement) however leads to a constant reduction in E, indicating enhanced corrosion.

alt-text: Fig. 17

Fig. 17
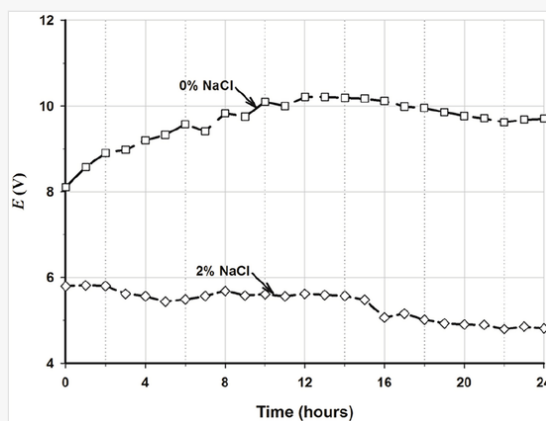
Test 5.1 results: effect of chloride contents on the ability that discrete steel fibre to pick up stray AC currents ($I_0 = 10mA; \ \omega = 50 \ Hz$).

After **test 4.1**, steel fibre specimens were rinsed with deionized water and EIS (**test 4.2**) was conducted to determine their corrosion states after AC polarization. EIS results were presented as the Bode phase plot (Fig. 18 (a)), Bode |Z| plot (Fig. 18 (b)) and Nyquist plot (Fig. 18 (c)). The Bode phase plot allows the phase shift angle (θ) to be plotted in comparison to the excitation frequency (Hz) on a logarithmic scale. Fig. 18 (a) shows that the phase angle (θ) drops constantly at low EIS frequencies until the lowest value (valley) is reached at an excitation frequency of between 1 and 10 Hz, indicating the rate of charge transfer increases and the mass transfer has become a key parameter governing the corrosion rate. A rust layer might have formed on the steel fibre surface and the speed of the corrosion reactions is governed by the diffusion speed through the rust layer in such circumstances [34].
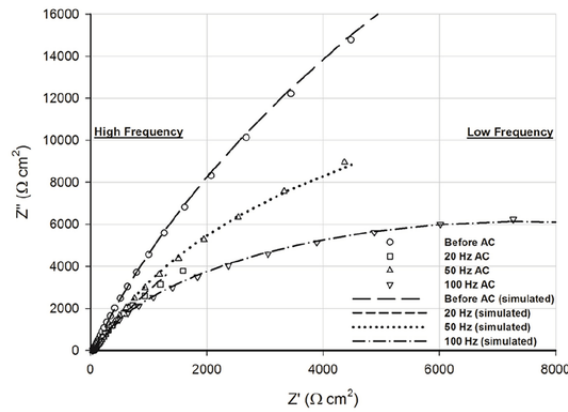
alt-text: Fig. 18

Fig. 18
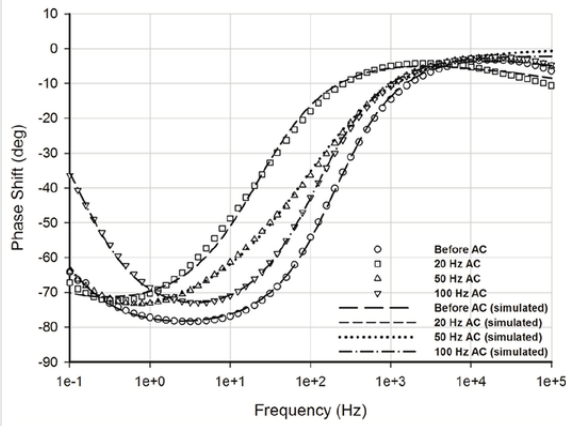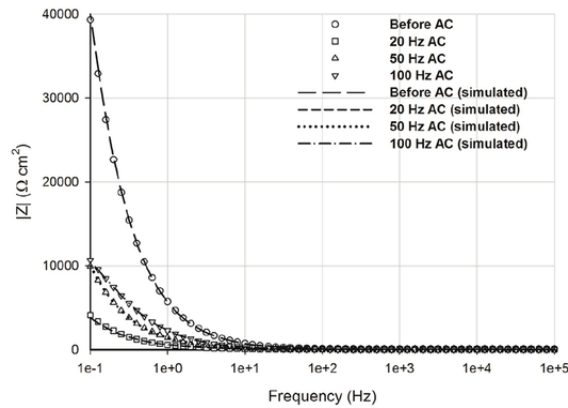
Test 4.2 results: effect of AC interference on EIS results (aqueous electrolyte).

Fig. 18 (b), the Bode $|Z|$ plot, shows that $|Z|$ at the low excitation frequency drops significantly from approximate 40,000 Ω cm^2 before AC polarization to less than 5000 Ω cm^2 after 1-hr 20 Hz AC polarization. The detrimental effect of 50 and 100 Hz AC on $|Z|$ was however smaller: $|Z|$ obtained at the low excitation frequency was about 10,000 Ω cm^2. In the Bode $|Z|$ plot, $|Z|$ obtained at the high EIS frequency (10^5 Hz) represents the bulk resistance of the solution (R_s) which is less than 50 Ω cm^2. This finding agrees with the

Nyquist plot (Fig. 18 (c)): the real impedance (Z') within the high frequency region (10^5 Hz) is less than 50 Ω cm^2 which can be attributed to the low solution resistance (R_s) aqueous electrolyte used. On the other hand, only one arc is shown in the Nyquist plot. Saremi and Mahallati [35] also observed a second arc in the Nyquist plot at high frequencies, attributing to the absorption of OH^- ions on the steel surface process. The second arc is not observed in Fig. 18 (c) and this can be attributed to the dislodgement effect that OH^- ions absorbed on the steel surface were gradually displaced by Cl^- ions in the electrolyte (i.e. 0.3 mol/L NaCl). At low frequency regions, an independent arch representing the oxide layer residing on the steel fibre surface, as reported by Torrents et al. [36] and Ozyurt et al. [37], is not identified either and this can be attributed to the small resistance of steel passivation layer. During EIS, the absorption effect (OH^- ions) at high frequencies and transfer resistance govern the impedance while diffusion normally determines impedance at low frequencies. As these processes are coupled, it is difficult to distinguish them based on the frequency ranges. In this work, EIS data were interpreted by fitting them to an equivalent electrical circuit model (Fig. 19). In this equivalent circuit, the bulk resistance of the electrolyte was represented by a resistor (R_s) and it is in series to a parallel connection of charge transfer resistance (R_{ct}) and double layer capacitance (C_{dl}). R_{ct} represents the Faradaic reactions which occur on the electrode (steel) surface. C_{dl} represents all non-Faradaic charge storage processes and is modelled as a constant phase element (CPE), considering the surface roughness and heterogeneousness of a double layer better [16]. Best-fit curves based on the equivalent electronic circuit modelling are shown in Fig. 18 and they match very well with the measured EIS data. EIS best-fit results are also presented in Table 2. A reduction in AC frequencies (ω) leads to a reduction in R_{ct} and thus reduces corrosion resistance and this finding agrees with Eq. (10). Table 2 also shows that C_{dl} exceeds 100×10^{-6} S·s^n·cm^{-2} after low frequency AC interference, i.e. 20 and 50 Hz. This indicates general corrosion has occurred on the steel surface [35].

alt-text: Fig. 19

Fig. 19
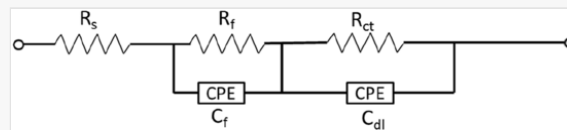
EIS equivalent electrical circuit used to model **test 4.2** and **5.2**.

alt-text: Table 2

Table 2

> (i) The presentation of Tables and the formatting of text in the online proof do not match the final output, though the data is the same. To preview the actual presentation, view the Proof.
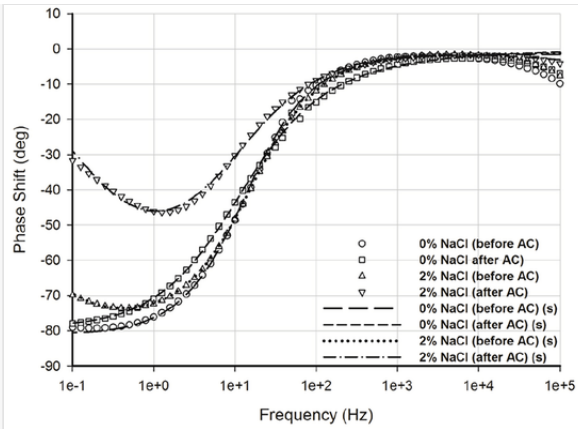
Test 4.2 results: effect of AC interference on EIS best-fit results (aqueous electrolyte).

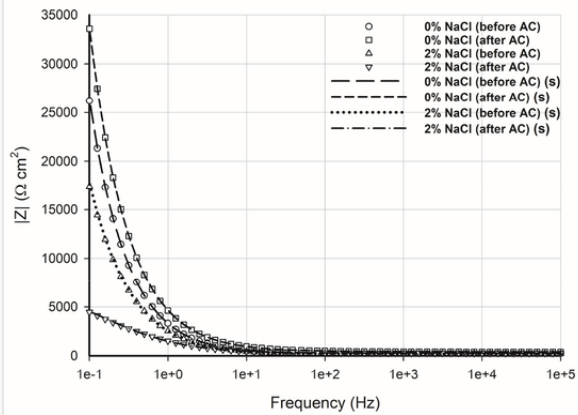|	OCP (mV)	R_s ($\Omega \cdot cm^2$)	R_f ($\Omega \cdot cm^2$)	C_f (10^{-6} S·s^n·cm^{-2})	n_f	R_{ct} (k$\Omega \cdot cm^2$)	C_{dl} (10^{-6} S·s^n·cm^{-2})	n_{dl}
Before AC	−268	14.0	35.8	25.5	0.41	129.6	34.0	0.89
After 20 Hz AC	−426	1.0	47.1	499.7	0.24	29.6	371.6	0.84
After 50 Hz AC	−418	33.2	97.4	998.7	0.60	35.7	140.8	0.89
After 100 Hz AC	−484	25.8	14.9	85.6	0.87	125.0	51.9	0.75

After **test 5.1**, EIS (i.e. **test 5.2**) was conducted to the SFRC specimens. EIS results are presented as the Bode phase plot (Fig. 20 (a)), Bode $|Z|$ plot (Fig. 20 (b)) and Nyquist plot (Fig. 20 (c)). Fig. 20 (a) shows that the phase angle (θ) drops gradually at low frequencies, especially under a combined effect of NaCl and AC interference which shifts θ downwards drastically. This indicates that the steel passive layer has been locally destroyed and the diffusion process might become a governing factor which controls the overall corrosion speed [34]. Fig. 20 (a) also shows that the Bode Phase plots are very similar to those obtained using aqueous electrolytes (Fig. 18 (a)). As a result, the same equivalent circuit (Fig. 19) was used to model the corrosion processes experienced by the steel fibres embedded in mortar. In the Bode $|Z|$ plot (Fig. 20 (b)), steel membrane resistance (R_f) and charge transfer resistance (R_{ct}) govern the total impedance ($|Z|$) at low frequencies while R_s is primarily related to the impedance obtained at high frequencies. $|Z|$ observed at a high excitation frequency of 10^5 Hz shows greater solution resistance (R_s) in comparison to that of the simulated concrete pore solutions. This has been confirmed by the best-fit results as seen in Table 3: R_s is much bigger than those shown in Table 2. Table 3 also shows that membrane resistance (R_f) is much bigger than those obtained using aqueous electrolytes (Table 2), indicating that the formation of corrosion products is more rapid in the solid electrolyte [38]. R_{ct} obtained under a chloride-free condition (0% NaCl) is over 2000 kΩ cm^2, which is more than one order of magnitude higher than those obtained using aqueous electrolytes. As R_{ct} is inversely proportional to the CR, an enhanced corrosion resistance is expected due to the use of mortar as the electrolyte. The combined effect of 2% NaCl (by mass of cement) and AC interference however has a significant detrimental effect on the corrosion resistance of steel fibres: R_{ct} reduces by two orders of magnitude, indicating high corrosion susceptibility. It should be noted that R_{ct} alone might not be sufficient to define the corrosion resistance under an AC environment due to the electrical double layer developed on the steel surface and its electrical performance, as defined as C_{dl}, also significantly affects the amount of electric charge transferred. Table 3 shows that C_{dl} is 183.8×10^{-6} S·s^n·cm^{-2} after 24-hr AC interference, indicating that general corrosion has occurred on the steel surface [35]. As the charge transfer resistance (R_{ct}) is much bigger than R_f, only one time constant is obvious in the Bode Phase plot (Fig. 20 (a)).
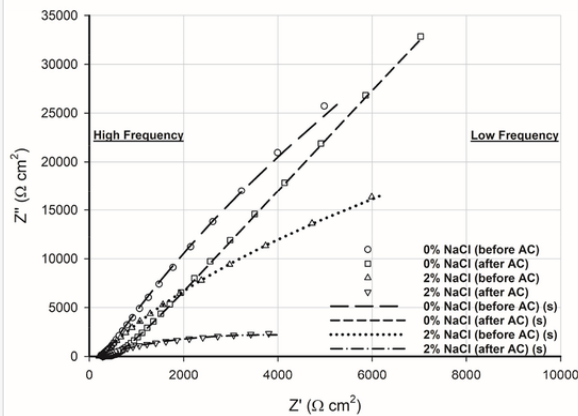
alt-text: Fig. 20

Fig. 20

(a) Bode Phase plot

(b) Bode Z plot

(c) Nyquist plot

Test 5.2 results: effect of AC interference on EIS results (solid electrolyte).

ⓘ The presentation of Tables and the formatting of text in the online proof do not match the final output, though the data is the same. To preview the actual presentation, view the Proof.

Test 5.2 results: effect of AC interference on EIS best-fit results (solid electrolyte).

	OCP (mV)	R_s ($\Omega\cdot cm^2$)	R_f ($\Omega\cdot cm^2$)	C_f ($10^{-6} S\cdot s^n\cdot cm^{-2}$)	n_f	R_{ct} ($k\Omega\cdot cm^2$)	C_{dl} ($10^{-6} S\cdot s^n\cdot cm^{-2}$)	n_{dl}
0% NaCl (before AC)	−274	250	2746	2671	0.19	2157.0	58.0	0.91
0% NaCl (after AC)	−336	377	2143	837	0.36	3015.0	45.7	0.89
2% NaCl (before AC)	−269	151	66	3.4	0.58	142.0	82.6	0.27
2% NaCl (after AC)	−594	75	213	6.7	0.35	6.9	183.8	0.72

In summary, SFRC develops good corrosion resistance to AC interference under a chloride-free environment. Special attention is still needed for SFRC subject to high concentration chloride, e.g. $\geq 2\%$ NaCl (by mass of cement). This work also shows that the 50 Hz AC, which is same as the National Grid AC frequency as used in electrified railway, has a detrimental effect on the corrosion resistance of SFRC.

3.4 Future work – durability design of SFRC under stray current environments

A conventional stray-current corrosion monitoring system normally involves the measurement of rail-to-earth resistance and/or the corrosion potential (E_{corr}) of the railway infrastructures including station platforms, retaining walls and tunnels [39]. These measurements however cannot provide sufficient information about the real-life steel reinforcement corrosion state as discussed in this paper. As a result, it is not unusual that serious stray-current induced corrosion is only identified through visual inspection and even by changes in train ride quality which can lead to a serious train delay and even cancellation for emergency maintenance work. There is scope to put this research into a wider context: to develop durability design guideline for SFRC under stray current environments and a real-time transit structure health monitoring system. An example of a probabilistic design approach for the service life design of a railway tunnel is shown below:

Previous Version

$$p\{\} = p_{dep.} = p\left\{C_{crit} - C\left(a, t_{SL}\right) < 0 \text{ or } i_{crit} - i_a < 0\right\}$$

Updated Version

$$p\{\} = p\left\{C_{crit} - C\left(a, t_{SL}\right) < 0 \text{ or } i_{crit} - i_a < 0\right\}$$

Eq. (11)

$p\{\ \}$: Probability that steel depassivation occurs;

C_{crit}: Critical chloride content (% by mass of cement or mol/L of chloride ions in the concrete pore solution);

$C(a, t_{SL})$: Chloride content at depth a at time t (% by mass of cement or mol/L of chloride ions in the concrete pore solution);

i_{crit}: Critical stray current density (mA/cm^2);

i_a: Anodic current density (mA/cm^2).

4 Conclusion

Analytical and experimental results discussed in this work show that stray AC currents can be picked up and transferred by discontinuous steel reinforcement. The severity of corrosion depends on the AC current density, angular frequencies (ω), the electrochemical properties of the electrodes (e.g. polarization resistance) and chloride contents. The mathematical solution (Eq. (10)) obtained through electrochemical modelling and numerical simulation allows a quantitative assessment of steel corrosion severity by determining the Faradaic current (I_2) which is directly related to the steel dissolution speed.

The use of discontinuous reinforcement such as steel fibres has a mitigation effect on stray AC induced corrosion in comparison to conventional steel reinforcement. This is due to the electrical double layer developed on the surface which reduces the Faradaic current (I_2) transferred by the discrete steel fibre. On the other hand, a reduced AC potential gradient is required to push electrons through discontinuous reinforcement under a higher chloride condition ($\geq$2% NaCl by mass of cement). Special attention is therefore required for SFRC used under a high chloride level in the presence of stray AC currents.

Acknowledgements

Appendix

Fig. 16 represents the steel-concrete interfacial electrochemical reactions under an stray AC environment. The AC current ($I = I_0 \cdot \sin \omega t$) causes an identical voltage drop across R_{ct} and C in a parallel circuit. The circuit containing R_{ct}, C and R_s is in a parallel arrangement with mortar bulk resistance (R_b), leading to the same voltage drop. The sum of the currents through each path, i.e. I_1, I_2 and I_3, is equal to the total current (I). The above processes are represented as:

$$R_{ct} \cdot I_2(t) = \frac{1}{C} \int I_1 dt$$

(A1)

$$R_b \cdot I_3\,(t) = R_s \cdot \left[I_1\,(t) + I_2\,(t) \right] + R_{ct} \cdot I_2\,(t)$$

(A2)

$$I_1\,(t) + I_2\,(t) + I_3\,(t) = I = I_0 \cdot \sin\,\omega t$$

(A3)

Taking differentiation with respect to t, Eq. (A1) becomes:

$$R_{ct} \cdot I_2'\,(t) = \frac{I_1}{C}$$

(A4)

Eq. (A4) can be written as:

$$I_1\,(t) = C \cdot R_{ct} \cdot I_2'\,(t)$$

(A5)

In conjunction with Eq. (A2) and (A3), $I_2\,(t)$ can be presented as:

$$C \cdot R_{ct} \cdot I_2'\,(t) + I_2\,(t) + \frac{R_s}{R_b}\left[I_1\,(t) + I_2\,(t) \right] + \frac{R_{ct}}{R_b} \cdot I_2\,(t) = I_0 \cdot \sin\,\omega t$$

(A6)

Eq. (A6) can be written as:

$$I_2'\,(t) + \frac{R_b + R_s + R_{ct}}{C \cdot R_{ct} \cdot R_b + R_s \cdot C \cdot R_{ct}} I_2\,(t) = \frac{R_b \cdot I_0}{C \cdot R_{ct} \cdot R_b + R_s \cdot C \cdot R_{ct}}\,\sin\,\omega t$$

(A7)

Eq. (A7) is shown below as a nonhomogeneous ordinary differential equation (ODE):

$$y' + a \cdot y = b\,\sin\,\omega t$$

(A8)

where $y = I_2\,(t)$, $a = \frac{R_b + R_s + R_{ct}}{C \cdot R_{ct} \cdot R_b + R_s \cdot C \cdot R_{ct}} I_2$ and $b = \frac{R_b \cdot I_0}{C \cdot R_{ct} \cdot R_b + R_s \cdot C \cdot R_{ct}}$.

Eq. (A9) represents a special case of Eq. (A8), in a homogeneous ODE format:

$$y' + a \cdot y = 0$$

(A9)

Eq. (A9) can be written as:

$$\frac{dy}{y} = -a \cdot dt$$

(A10)

By integration:

$$lny = -at + lnc$$

(A11)

where c is the constant of integration. Taking exponents on both sides

$$y = ce^{-at}$$

(A12)

Let $c = u(t)$ and Eq. (A12) becomes

$$y = u(t) \cdot e^{-at}$$

(A13)

Taking differentiation on both sides

$$y' = u'(t) \cdot e^{-at} - a \cdot u(t) \cdot e^{-at}$$

(A14)

Substitution of Eq. (A13) and (A14) into (A8):

$$u' = b \cdot e^{at} \cdot \sin \omega t$$

(A15)

By integration:

$$u = b \int e^{at} \cdot \sin \omega t dt + c$$

(A16)

where c is the constant of integration. Taking integration by parts, Eq. (A16) can be solved as

$$u = \frac{b \cdot e^{at}}{\omega^2 + a^2} (a \cdot \sin \omega t - \omega \cdot \cos \omega t) + c$$

(A17)

By substituting Eq. (A17) into (A13), the general solution of Eq. (A8) is:

$$y = \frac{b}{\omega^2 + a^2} (a \cdot \sin \omega t - \omega \cdot \cos \omega t) + c \cdot e^{-at}$$

(A18)

Applying the initial condition, $y|_{t=0} = 0$, c can be solved as:

$$c = \frac{b \cdot \omega}{\omega^2 + a^2}$$

(A19)

Eq. (A18) therefore becomes:

$$y = \frac{b}{\omega^2 + a^2} (a \cdot \sin \omega t - \omega \cdot \cos \omega t) + \frac{b \cdot \omega}{\omega^2 + a^2} \cdot e^{-at}$$

(A20)

Eq. (A20) can be further simplified as

$$y = \frac{b}{\sqrt{\omega^2 + a^2}} \sin (\omega t - \theta) + \frac{b \cdot \omega}{\omega^2 + a^2} \cdot e^{-at}$$

(A21)

where $\theta = arctan\frac{\omega}{a}$, the phase drift (rads).

As $y = I_2(t)$, the solution of the initial problem is:

$$I_2(t) = \frac{b}{\sqrt{\omega^2 + a^2}} \sin(\omega t - \theta) + \frac{b \cdot \omega}{\omega^2 + a^2} \cdot e^{-at}$$

(A22)

where: $a = \frac{R_b + R_s + R_{ct}}{C \cdot R_{ct} \cdot R_b + R_s \cdot C \cdot R_{ct}}$, $b = \frac{R_b \cdot I_0}{C \cdot R_{ct} \cdot R_b + R_s \cdot C \cdot R_{ct}}$, $\theta = arctan\frac{\omega}{a}$.

The validity of Eq. (A22) was assessed using standard resistors (R_s and R_{ct}) and capacitors (C). AC current $I_0 \cdot \sin \omega t$ ($I_0 = 10\ mA$; $f = 50Hz$; $\omega = 2\pi f$) was swept through this circuit using the Gamry galvanostat. The potential drop through R_{ct} was captured by the galvanostat to calculate I_2 according to Ohm's law. The predicted I_2 according to Eq. (A22) was in good agreement with the experimental measurements as seen in Fig. 21. Fig. 21 (a) and (b) also depicts that a reduction in AC frequencies (ω), R_{ct} or C will lead to an increase in I_2, or more serious corrosion in embedded steel.

alt-text: Fig. 21

Fig. 21
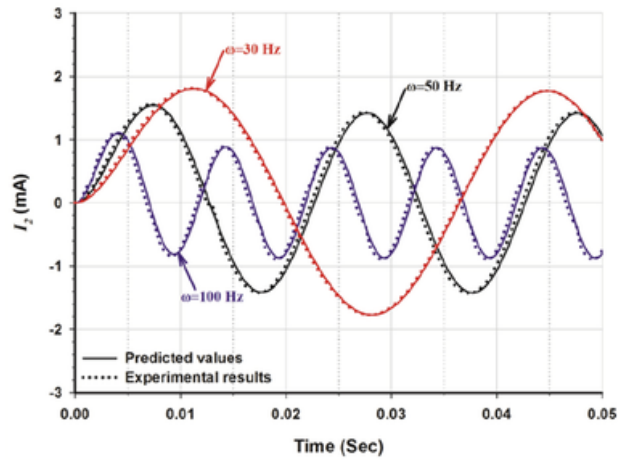
(a) Effect of ω on I_2 ($R_{ct} = 1000\Omega$; $R_s = 220\Omega$; $R_b = 330\Omega$; $C = 10\mu F$)
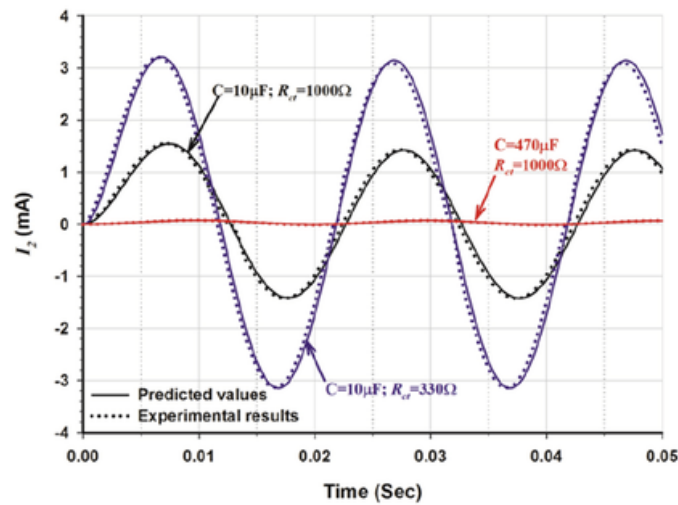
(b) Effect of R_{ct} and C on I_2 ($\omega = 50Hz$; $R_s = 220\Omega$; $R_b = 330\Omega$)

Validation of Eq. (10) – predicted and measured I_2 [Instruction: Fig. 21 appears to be too big and the PDF proof does not shall the whole captions of Fig. 21 (a) and (b). Can the figure sizes be reduced a bit to show the entire text? Thank you!]

References

[1] Jovičić V., Šušteršič J., Use of fibre-reinforced shotcrete for primary lining in the Dekani tunnel, Quark, Summer (2008) 112–117.

[2] Greenhalgh J., 20 Years of Fibre Concrete Linings in the UK, 2010.

[3]

Burgess M., Davies H., Channel tunnel rail link section 2: thames tunnel, Proc. Inst. Civ. Eng. Civ. Eng. 160 (2007) 14–18.

[4] Tang K., Stray current induced corrosion to steel fibre reinforced concrete, Cement Concr. Res. 100 (2017) 445–456.

[5] BSI, BS EN 50122-2:2010 Railway Applications - Fixed Installations - Electrical Safety, Earthing and the Return Circuit, British Standards Institution, 2010.

[6] Prinz W., AC induced corrosion on cathodically protected pipelines, UK Corrosion '92, Sandown Park, England, 1992.

[7] Ragault I., Electrical lines on polyethylene coated steel gas pipelines, CORROSION 98, NACE International, San Diego, California, USA, 1998.

[8] Wakeling R.G., Gummow R.A., Segall S.M., AC corrosion - case history, test procedures & mitigation, CORROSION 98, NACE International, San Diego, California, USA, 1998.

[9] Bertolini L., Carsana M., Pedeferri P., Corrosion behaviour of steel in concrete in the presence of stray current, Corrosion Sci. 49 (2007) 1056–1068.

[10] Kuang D., Cheng Y.F., Understand the AC induced pitting corrosion on pipelines in both high pH and neutral pH carbonate/bicarbonate solutions, Corrosion Sci. 85 (2014) 304–310.

[11] Hanson H.R., Smart J., AC corrosion on a pipeline located in a HVAC utility corridor, Corrosion, NACE International, Louisiana, New Orleans, 2004.

[12] Figueira R.B., Sadovski A., Melo A.P., Pereira E.V., Chloride threshold value to initiate reinforcement corrosion in simulated concrete pore solutions: the influence of surface finishing and pH, Construct. Build. Mater. 141 (2017) 183–200.

[13] Brenna A., Beretta S., Bolzoni F., Pedeferri M., Ormellese M., Effects of AC-interference on chloride-induced corrosion of reinforced concrete, Construct. Build. Mater. 137 (2017) 76–84.

[14] Bertolini L., Corrosion of Steel in Concrete Prevention, Diagnosis, Repair, second ed., Wiley-VCH, Weinheim, Germany, 2013.

[15] Tang K., Corrosion of steel fibre reinforced concrete (SFRC) subjected to simulated stray direct (DC) interference, Mater. Today. Commun. (2019) 100564.

[16] Ye C.Q., Hu R.G., Dong S.G., Zhang X.J., Hou R.Q., Du R.G., Lin C.J., Pan J.S., EIS analysis on chloride-induced corrosion behavior of reinforcement steel in simulated carbonated concrete pore solutions, J. Electroanal. Chem. 688 (2013) 275–281.

[17] Pourbaix M., Lectures on Electrochemical Corrosion, Plenum Press, NY, USA, 1973.

[18]

Andrade C., Alonso C., Corrosion rate monitoring in the laboratory and on-site, Construct. Build. Mater. 10 (1996) 315–328.

[19] Brenna M., Dolara A., Leva S., Zaninelli D., Effects of the DC stray currents on subway tunnel structures evaluated by FEM analysis, IEEE PES General Meeting, PES 2010, July 25, 2010 - July 29, 2010, IEEE Computer Society, Minneapolis, MN, United states, 2010.

[20] Hong Y., Li Z., Qiao G., Ou J., Numerical simulation and experimental investigation of the stray current corrosion of viaducts in the high-speed rail transit system, Construct. Build. Mater. 157 (2017) 416–423.

[21] Laurens S., Hénocq P., Rouleau N., Deby F., Samson E., Marchand J., Bissonnette B., Steady-state polarization response of chloride-induced macrocell corrosion systems in steel reinforced concrete — numerical and experimental investigations, Cement Concr. Res. 79 (2016) 272–290.

[22] Patil S., Karkare B., Goyal S., Corrosion induced damage detection of in-service RC slabs using acoustic emission technique, Construct. Build. Mater. 156 (2017) 123–130.

[23] Sadeghi-Pouya H., Ganjian E., Claisse P., Muthuramalingam K., Corrosion durability of high performance steel fibre reinforced concrete, in: Peter Claisse T.N. (Ed.), The 3rd International Conference on Sustainable Construction Materials and Technologies, Kyoto, Japan, 2013.

[24] Duranceau S.J., Johnson W.J., Pfeiffer-Wilder R.J., A study examining the effect of stray current on the integrity of continuous and discontinuous reinforcing bars, Exp. Tech. 35 (2011) 53–58.

[25] Wang K., Wu Q.S., Chen M.C., Xie L., Corrosion fatigue of reinforced concrete in the presence of stray current, 2011 International Conference on Electric Technology and Civil Engineering (ICETCE), 2011, pp. 1133–1136.

[26] Li W., The monitor and control system of stray current corrosion in metro, Urban Mass Transit 6 (2003) 48–52.

[27] Wikipedia, Seawater, https://en.wikipedia.org/wiki/Seawater (accessed 1/8/2019), SeawaterWikipedia, 2019.

[28] Kasper T., Edvardsen C., Wittneben G., Neumann D., Lining design for the district heating tunnel in Copenhagen with steel fibre reinforced concrete segments, Tunn. Undergr. Space Technol. 23 (2008) 574–587.

[29] Helmenstine A.M., Table of Electrical Resistivity and Conductivity, https://www.thoughtco.com/table-of-electrical-resistivity-conductivity-608499 (accessed October 23, 2018), Table of Electrical Resistivity and ConductivityThoughtCo., 2018.

[30] Gamry, Gamry Echem Analyst in, Gamry Instruments, Inc., 2015.

[31]

Wang X., Liu Q., Chun Y., Li Y., Wang Z., Evaluation of delamination of X80 pipeline steel coating under alternating stray current via scanning electrochemical microscopy, J. Mater. Eng. Perform. 27 (2018) 3060–3071.

[32] Wikipedia, ~~Skin Effect~~Skin effect, https://en.wikipedia.org/wiki/Skin_effect (accessed 23/10/2019), Wikipedia, ~~2018~~2019.

[33] Tang K., Wilkinson S., Beattie G., Effects of curing temperature on the hydration of GGBS blended concrete and the use of electron microscope particle analysis, Adv. Cement Res. 29 (2017) 322–335.

[34] Wei J., Fu X.X., Dong J.H., Ke W., Corrosion evolution of reinforcing steel in concrete under dry/wet cyclic conditions contaminated with chloride, J. Mater. Sci. Technol. 28 (2012) 905–912.

[35] Saremi M., Mahallati E., A study on chloride-induced depassivation of mild steel in simulated concrete pore solution, Cement Concr. Res. 32 (2002) 1915–1921.

[36] Torrents J.M., Mason T.O., Garboczi E.J., Impedance spectra of fiber-reinforced cement-based composites: a modeling approach, Cement Concr. Res. 30 (2000) 585–592.

[37] Ozyurt N., Mason T.O., Shah S.P., Non-destructive monitoring of fiber orientation using AC-IS: an industrial-scale application, Cement Concr. Res. 36 (2006) 1653–1660.

[38] Yang Z.X., Kan B., Li J.X., Su Y.J., Qiao L.J., Hydrostatic pressure effects on corrosion behavior of X70 pipeline steel in a simulated deep-sea environment, J. Electroanal. Chem. 822 (2018) 123–133.

[39] Szeliga M.J., Stray Current Corrosion: the Past, Present, and Future of Rail Transit Systems, NACE International Philadelphia, USA, 1994.

Queries and Answers

Query: Your article is registered as a regular item and is being processed for inclusion in a regular issue of the journal. If this is NOT correct and your article belongs to a Special Issue/Collection please contact n.thandavamoorthy@elsevier.com immediately prior to returning your corrections.
Answer: Yes

Query: Please confirm that given names and surnames have been identified correctly and are presented in the desired order and please carefully verify the spelling of all authors' names.
Answer: Yes.